Climate-driven ground-level ozone extreme in the fall over the Southeast United States

Yuzhong Zhang[a] and Yuhang Wang[a,1]

[a]School of Earth and Atmospheric Sciences, Georgia Institute of Technology, Atlanta, GA 30332

Edited by A. R. Ravishankara, Colorado State University, Fort Collins, CO, and approved July 11, 2016 (received for review February 15, 2016)

Ground-level ozone is adverse to human and vegetation health. High ground-level ozone concentrations usually occur over the United States in the summer, often referred to as the ozone season. However, observed monthly mean ozone concentrations in the southeastern United States were higher in October than July in 2010. The October ozone average in 2010 reached that of July in the past three decades (1980–2010). Our analysis shows that this extreme October ozone in 2010 over the Southeast is due in part to a dry and warm weather condition, which enhances photochemical production, air stagnation, and fire emissions. Observational evidence and modeling analysis also indicate that another significant contributor is enhanced emissions of biogenic isoprene, a major ozone precursor, from water-stressed plants under a dry and warm condition. The latter finding is corroborated by recent laboratory and field studies. This climate-induced biogenic control also explains the puzzling fact that the two extremes of high October ozone both occurred in the 2000s when anthropogenic emissions were lower than the 1980s and 1990s, in contrast to the observed decreasing trend of July ozone in the region. The occurrences of a drying and warming fall, projected by climate models, will likely lead to more active photochemistry, enhanced biogenic isoprene and fire emissions, an extension of the ozone season from summer to fall, and an increase of secondary organic aerosols in the Southeast, posing challenges to regional air quality management.

ground-level ozone | ozone season | regional climate change | isoprene | air quality

Ground-level ozone is a pollutant harmful to human and vegetation health (1, 2). High ground-level ozone events are typically found in the summer when the formation of ozone is active through photochemical reactions involving nitrogen oxides (NO_x = NO + NO_2) and volatile organic compounds (VOCs). However, ozone concentrations are sensitive to weather and climate (3–8), and the high-ozone season could extend beyond summer in the future (9–13). Previous climate-chemistry model studies have estimated the change of ground-level ozone (ΔO_3) in the United States resulting only from meteorological changes. Their results show large variation in the sign and magnitude of ΔO_3 in the fall, especially over forested regions such as the southeastern United States (SE) (10, 13). The lack of consensus reflects the uncertainties in modeling regional climate change and the consequent response of ground-level ozone.

In this study, we focus on analyzing the historical ozone records. Fig. 1*A* shows the surface observations of monthly mean maximum daily 8-h average ozone concentration ($[O_3]_{MDA8}$) in October 2010. The regional $[O_3]_{MDA8}$ concentrations were higher than all other regions of the United States except a small area in southern California. There were 133 exceedances with daily $[O_3]_{MDA8}$ values greater than 75 parts per billion by volume (ppbv) at 66 stations in the SE (*SI Appendix*, Fig. S1). The number increases to 324 exceedances at 112 stations if the new US ambient ozone standard threshold value, 70 ppbv, is used (*SI Appendix*, Fig. S1). The regional average reached 65 ppbv during October 8–10, 2010 (Fig. 2*A*).

Fig. 1*B* puts the 2010 observations in the context of regional monthly mean $[O_3]_{MDA8}$ in October over the SE in the past three decades. The 30-y climatology mean of $[O_3]_{MDA8}$ in October is ∼40 ppbv, considerably lower than that in the summer ozone season (∼50 ppbv in July). However, in the two extreme years, 2000 and 2010, regional monthly mean $[O_3]_{MDA8}$ are 52 and 49 ppbv, respectively, two interannual standard deviations higher than the climatological mean. There is no obvious ozone trend over the SE in October in the last three decades, in contrast to the significant decrease of $[O_3]_{MDA8}$ in the summer since the 1980s (Fig. 1*B*), suggesting that either ozone concentrations are insensitive to the large emission decreases in the past three decades (14) (*SI Appendix*, Fig. S2) or the emission reduction benefit is diminished by regional climate change. In this study, we apply statistical and regional model simulations to understand the high ozone extreme in October 2010. Model simulations are conducted for 2008, 2009, and 2010, which have low extreme, average, and high extreme October SE ozone concentrations in the last 30 y.

Results and Discussion

Strong Correlation Between Ozone and Humidity. Observation-based statistical analysis shows that surface ozone is affected by a number of meteorological factors, including temperature, humidity, surface pressure, wind speed, and wind direction (8, 11, 15, 16). Correlations between surface ozone and these meteorological parameters vary with region and season, but temperature is usually found to best correlate with ozone in the summer (8, 16). In October over the SE, using the monthly mean data from 1980 to 2010, we find that the correlation of $[O_3]_{MDA8}$ with daily maximum temperature (T_{max}, $R^2 = 0.16$) is much lower than with two humidity measures, daytime relative humidity (RH; $R^2 = 0.68$) and vapor pressure deficit (VPD; defined as the difference between saturation vapor pressure and ambient vapor pressure, $R^2 = 0.67$) (Fig. 3 *A* and *B*). Hereafter, we use daytime VPD in this study because it is directly related to water stress of plants (17, 18). Using daily data, the

Significance

High ozone concentrations usually occur in the summer over the United States. However, in extreme cases, such as October 2010 over the southeast United States, ozone during the fall reached the summer level. We find a large contribution by enhanced emissions of biogenic isoprene to ozone extremes from water-stressed plants under a drying and warming condition. This finding also explains the puzzling fact that the two extremes of high October ozone over the region all occurred in the 2000s, with lower anthropogenic emissions than the 1980s–1990s. We suggest that occurrences of a drying and warming fall in the future may lead to an extension of the ozone season from summer to fall, posing challenges to regional air quality management and public health.

Author contributions: Y.Z. and Y.W. designed research; Y.Z. performed research; Y.Z. and Y.W. analyzed data; and Y.Z. and Y.W. wrote the paper.

The authors declare no conflict of interest.

This article is a PNAS Direct Submission.

Freely available online through the PNAS open access option.

[1]To whom correspondence should be addressed. Email: ywang@eas.gatech.edu.

This article contains supporting information online at www.pnas.org/lookup/suppl/doi:10.1073/pnas.1602563113/-/DCSupplemental.

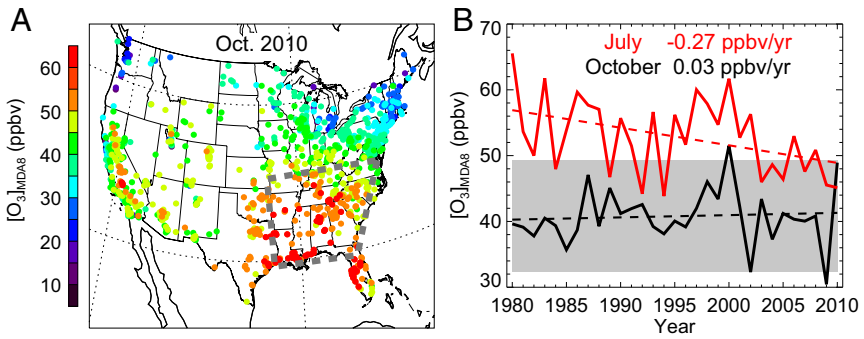

Fig. 1. Monthly mean $[O_3]_{MDA8}$ in October over the SE United States. (*A*) Observed monthly mean $[O_3]_{MDA8}$ distribution over the United States in October 2010. The gray dashed lines enclose the SE region for this study. Each dot denotes an observation site. (*B*) Regional-averaged monthly mean $[O_3]_{MDA8}$ over the SE in July (red solid line) and in October (black solid line) from 1980 to 2010. In contrast to the significant decreasing trend in July (red dashed), the trend in October (black dashed) is insignificant. In October 2000 and 2010, $[O_3]_{MDA8}$ reached 2 SDs (gray shading) above the climatology mean.

correlation of $[O_3]_{MDA8}$ with daytime VPD (R^2 = 0.66) is also much higher than with T_{max} (R^2 = 0.25) (*SI Appendix*, Fig. S3).

The interpretation of a linear correlation analysis is often complicated by the colinearity between meteorological factors resulting in part from the synoptic-scale weather (3, 11). We use the explained variance decomposition (EVD) method to analyze the variance contributions of T_{max} and daytime VPD to daily $[O_3]_{MDA8}$ in four regions, SE, Northeast (NE), Midwest (MW), and California (CA) during 1980–2010. We compare the explained variance (EV) of daily $[O_3]_{MDA8}$ attributable solely to T_{max} (EV_T) or daytime VPD (EV_{VPD}) and that attributable to the correlation between T_{max} and VPD ($EV_{T\text{-}VPD}$) in July and October (Fig. 3 *C* and *D*). These variables can explain 44–64% and 63–73% of the daily $[O_3]_{MDA8}$ variance in July and October, respectively. T_{max} driven EV_T is particularly large in NE, MW, and CA in July. $EV_{T\text{-}VPD}$ by the T_{max}-VPD correlation dominates in these regions in October and SE in July, i.e., we cannot tell if it is T_{max} or VPD or a combination of both that contributes to the EV of $[O_3]_{MDA8}$. The only case where EV_{VPD} dominates is in the SE in October with the rest of EV attributable to T_{max}-VPD correlation, implying that a VPD-related mechanism, possibly due to water stress-induced biogenic emissions (17–21), influences the ground-level ozone concentrations over the SE during the fall.

Recent work shows that the position of the west edge of the Bermuda High influences summer surface ozone in the eastern United States (22, 23). In October, the Bermuda High usually has weakened and retreated to the Eastern North Atlantic. However, we do find the variability of VPD over the SE during October is related to the presence of a high-pressure system. Using the 30-y reanalysis data, we find that daytime VPD is positively correlated

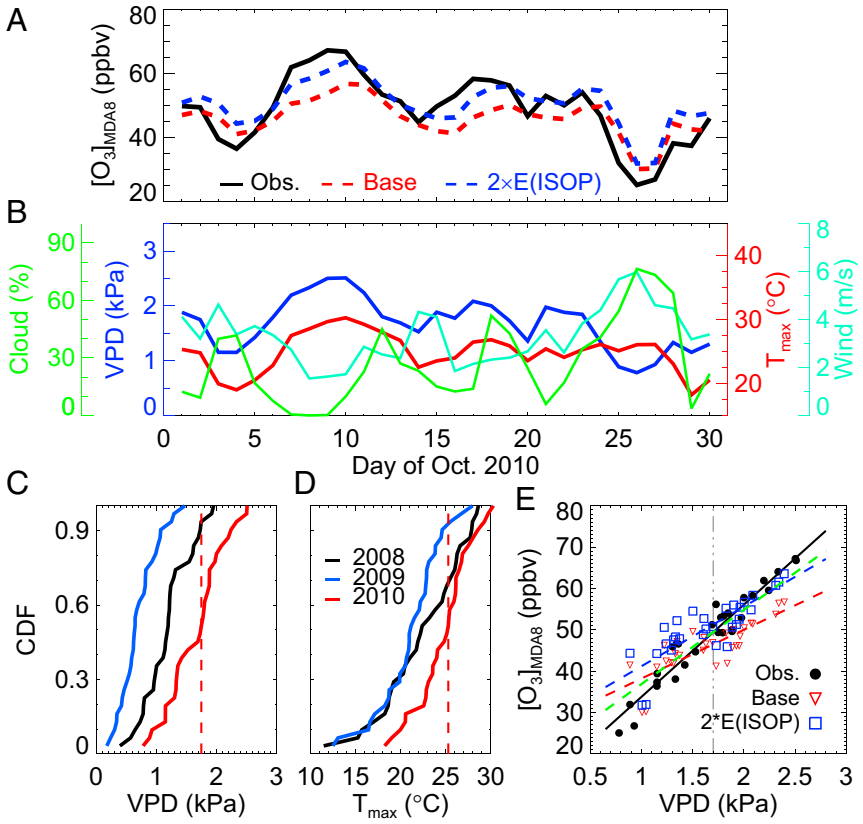

Fig. 2. High-ozone episodes in October 2010 over the SE. (*A*) Comparing with the observed regional-mean $[O_3]_{MDA8}$ (black solid), the base simulation (red dashed line) underestimates by ~15 ppbv during high-ozone episodes. The bias is greatly reduced in the simulation with doubled biogenic isoprene emissions (blue dashed line). (*B*) The ozone episodes are concurrent with high daytime VPD (i.e., dry conditions, blue), high temperature (red), low wind speed (cyan), and small cloud fraction (green). (*C* and *D*) The empirical cumulative distribution function (CDF) of daytime VPD (*C*) and T_{max} (*D*) in 2008 (black), 2009 (blue), and 2010 (red). The vertical red dashed line denotes the median values in October 2010. (*E*) Relationship between $[O_3]_{MDA8}$ and daytime VPD in observations (black), the base simulation (red), and the doubled isoprene emission simulation (blue). The green line represents linear regression using the base simulation when VPD < 1.7 kPa and the doubled isoprene emission simulation when VPD > 1.7 kPa.

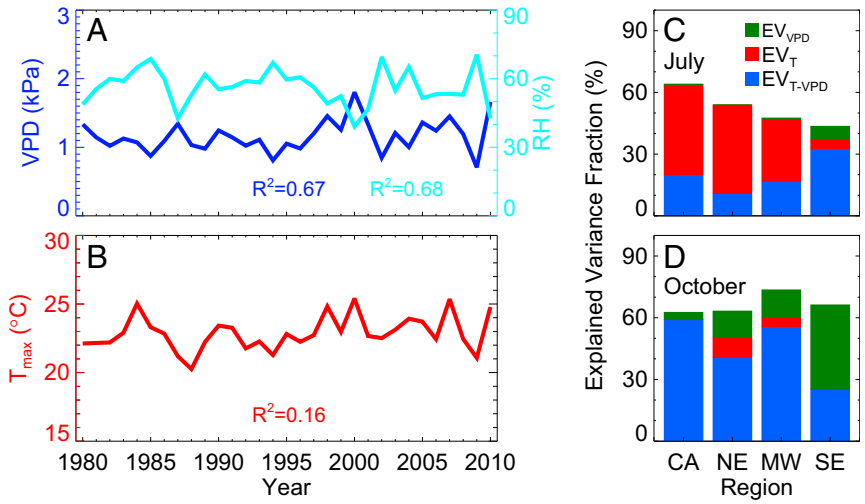

Fig. 3. Ground-level $[O_3]_{MDA8}$ and its relationship with meteorological variables in October from 1980 to 2010. (*A*) Monthly mean $[O_3]_{MDA8}$ is well correlated with monthly mean daytime (10:00 AM to 5:00 PM local time) VPD and RH in the SE. (*B*) Monthly mean $[O_3]_{MDA8}$ is correlated weakly with monthly mean T_{max} in the SE. (*C* and *D*) The explained variance fraction of daily $[O_3]_{MDA8}$ attributable to daily T_{max}, daytime VPD, and their correlations (T-VPD), respectively, for CA, NE, MW, and SE in July (*C*) and October (*D*).

with geopontential height at 850 hPa over the SE and clockwise surface wind around the region in October (*SI Appendix*, Fig. S4), suggesting that a mechanism similar to ref. 22 may affect the high VPD episodes observed during anomalous Octobers.

The Mechanism Contributing to Fall Ozone Extremes. To investigate the underlying mechanism leading to the correlated increase of VPD and surface ozone, we examine in detail the extreme monthly $[O_3]_{MDA8}$ in October 2010, when the ozone enhancement is regional in nature (Fig. 1*A*) and the SE regional mean is ~10 ppbv higher than the climatological mean (Fig. 1*B*). The ozone enhancement is mainly due to three episodes—October 7–12, 16–18, and 21–24—with concurrent high temperature and VPD (Fig. 2 *A* and *B*). We simulate the Octobers of 2008–2010 by using the Regional chEmical trAnsport Model (REAM) (24, 25) to examine the key parameters driving the surface ozone difference among the three years.

Fig. 2*A* shows that the base simulation underestimates $[O_3]_{MDA8}$ by ~15 ppbv during the three episodes in October 2010. The coupling between weather condition and surface ozone is clearly shown in Fig. 2*B*. During the period of warm and dry weather (i.e., high VPD values), ozone concentrations tend to be higher because fewer clouds (and no precipitation) increase photochemical production and a lower wind speed reduces ventilation of high ozone air mass by advection. However, these effects (e.g., cloud cover, see *SI Appendix*, Fig. S5) are already included in the base simulation. Meteorologically driven ozone variations in October 2008 and 2009 (e.g., surface ozone enhancements on Oct. 3, 2008, Oct. 20, 2008, and Oct. 20, 2009) are well simulated by the model (*SI Appendix*, Fig. S6). Thus, they are unlikely to be responsible for the underestimation of $[O_3]_{MDA8}$ in the base simulation in 2010.

We also find that the uncertainties in simulating the stratosphere-troposphere exchange are unlikely to be important for these ozone episodes in October 2010. Although the impact of stratospheric intrusion on surface ozone has been reported at elevated sites in the mountainous western United States (26–28), its effect on near-surface ozone in the eastern United States is insignificant (29), especially considering that stratospheric intrusion is weakest in the fall season (30, 31) (detailed discussion in *SI Appendix*, *SI Text*).

The coupling of weather and surface ozone is also a function of emissions. The ozone underestimation during dry and warm weather conditions may reflect errors in anthropogenic or natural emissions. We consider further that the model simulations do not have large biases when VPD values are low in October 2010 and that the model can simulate well the low-ozone October in 2009 and the average-ozone October in 2008 (*SI Appendix*, Fig. S6) when VPD values are considerably lower than 2010. It appears that anthropogenic emissions, which do not vary much with weather, are reasonably estimated in the model. Emissions from biomass burning are expected to be more intensive during a dry period. In fact, an examination of the Global Fire Emission Database (GFED4s) shows high fire emissions over the SE in October 2010, largely due to small fires (*SI Appendix*, Fig. S7). However, significant fire emissions affecting surface ozone are confined along the Mississippi Valley (*SI Appendix*, Fig. S7), in contrast to the observed ozone enhancements across the SE. Simulations show that the contribution of fire emissions to the regional average in the SE is <2 ppbv (*SI Appendix*, Fig. S7).

Another type of emission affected by weather is biogenic isoprene, which is the most significant VOC precursor for ground-level ozone in the eastern United States (32). Indeed, the large model biases of surface ozone in warm and dry weather are largely corrected in the sensitivity simulation in which model estimated isoprene emissions are doubled (Fig. 2 *A* and *E* and *SI Appendix*, Fig. S8). In addition, the increase in isoprene emissions also brings the model simulated column density of formaldehyde (CH_2O), a high-yield product from isoprene chemistry that is often used for validating the isoprene emission inventory (33, 34), to a better agreement with Global Ozone Monitoring Experiment-2 (GOME-2) satellite observations (*SI Appendix*, Fig. S9). Note that the CH_2O column in the base simulation agrees with GOME-2 observations in October 2008 and 2009. This comparison again indicates that the model most likely underestimated the isoprene emissions under the warm and dry weather of October 2010.

We did not perform sensitivity simulations with high-VDP enhanced isoprene emissions for October 2008 and 2009 because the available observations are inadequate to quantify the isoprene emission response function. However, if isoprene emission increase is a biological response of plants to short-term water stress (17–21), we would expect that there exists a threshold VPD value above which plants would respond. In fact, the base model underestimation of the observed ozone occurs mostly when daytime VPD is greater than its monthly median of 1.7 kPa (Fig. 2*E*). If we construct an $[O_3]_{MDA8}$ composite using the base simulation results when VPD < 1.7 kPa and the doubled isoprene emission

simulation when VPD > 1.7 kPa, the resulting regression slope (18 ppbv/kPa) between $[O_3]_{MDA8}$ and VPD is much closer to the observed regression slope (22 ppbv/kPa) than either the base simulation (12 ppbv/kPa) or the doubled isoprene emission simulation (14 ppbv/kPa) (Fig. 2*E*). Because no VPD values in 2008 and only ∼5% in 2009 exceeded 1.7 kPa (Fig. 2*C*), we expect that high-VPD driven isoprene emission enhancement is negligible in these two years. It is also noteworthy that compared with the large isoprene emissions (50–100 $mg{\cdot}m^{-2}{\cdot}d^{-1}$) in the summer over the SE (32), the doubled isoprene emissions in the sensitivity simulation (20–30 $mg{\cdot}m^{-2}{\cdot}d^{-1}$ for October 7–12 and ∼15 $mg{\cdot}m^{-2}{\cdot}d^{-1}$ for October 16–18 and 21–24 in 2010) are still quite low. However, because of the shift of chemistry regime from NO_x-sensitive in the summer to VOC-sensitive in the fall (35), the ozone production becomes more sensitive to isoprene emissions in October than July (Fig. 4 *A* and *B*). Therefore, it is important to accurately simulate biogenic isoprene emissions in the fall season.

The dependence of isoprene emissions on temperature is known, and the effect is already included in the-state-of-art biogenic emission algorithms (32). However, the base simulation (Fig. 2*A*) that includes this effect still underestimates regional mean $[O_3]_{MDA8}$ during the episodes and satellite CH_2O columns in October 2010. The sensitivity simulation with perturbed near surface temperature also shows that this effect alone is not large enough to explain the underestimation (*SI Appendix*, Fig. S10). Whereas 40% of daily T_{max} in 2009 exceeds the median T_{max} in 2010 (Fig. 2*D*), only 5% of 2009 daily VPD exceeds the 2010 median VPD (Fig. 2*C*). The response of isoprene emissions to VPD is studied much less and not included in current biogenic emission algorithms. Isoprene emissions decrease drastically under severe drought conditions when soil moisture is below a threshold (21, 32), confounding the relationship between isoprene emissions and VPD in field observations (20, 21, 36, 37). However, a few studies reported that the current biogenic emission algorithm underestimates the enhanced isoprene emissions at the initial stage of a drought when large variation in ambient humidity occurred but the decrease in soil moisture was insignificant (20, 21). Similarly, in the case of October 2010, high VPD was episodic (Fig. 2*B*) and soil moisture was not a limiting factor (*SI Appendix*, Fig. S11). In addition, a few laboratory studies have observed the enhancement of isoprene emissions in a dry environment (17–19). For example, controlling confounding factors such as air temperature, radiation, carbon dioxide concentration, soil moisture, and water vapor, a study conducted in Biosphere 2 found that the gross isoprene production from cottonwood trees is enhanced by a factor of 2 when VPD increased from 1 kPa to 3 kPa (17) (*SI Appendix*, Fig. S11), which is consistent with the doubling of isoprene emissions during high-ozone episodes of October 2010 (Fig. 2*B*). Enhanced isoprene emissions are likely due in part to increased leaf temperature and decreased internal CO_2 concentration, caused by reduced stomatal conductance under mild drought stress (20). More field and laboratory measurements are obviously required to quantify the response function of isoprene emission to short-term stress of high VPD and to understand the underlying mechanisms.

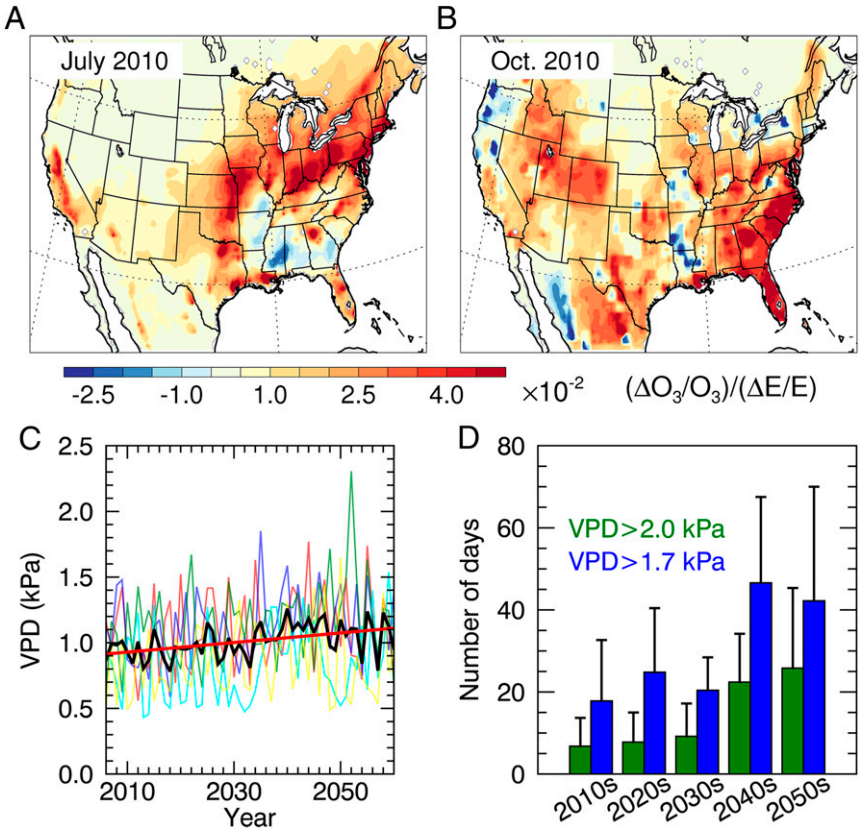

Fig. 4. Implications for air quality management. (*A* and *B*) Simulated relative sensitivity of daytime ozone to the change of isoprene emissions is larger in October 2010 (SE average 0.03) than in July 2010 (SE average 0.01) over the SE, demonstrating that the ozone production is more sensitive to biogenic VOC emissions in the fall because of the chemical regime shift. (*C*) Ensemble mean projection from the GFDL model (five ensemble members, RCP 4.5) shows an increasing trend of daytime VPD ($P < 0.01$) in the SE in October in the next 50 y. Thick black and red lines represent the ensemble mean and the linear trend, respectively. Thin colored lines are ensemble members. (*D*) Number of high VPD days similar to October 2010 episodes increase in the five GFDL model projections. Error bars represent the SD among the ensemble members.

Implications. The observations in the past three decades demonstrated that October ozone in the SE did not decrease like in July despite anthropogenic emission reductions in the region and that the two October high ozone extremes both occurred in the 2000s, implying higher ozone sensitivity to climate variation in October than July in the region. However, current discussion on the ozone climate penalty (the response of ground-level ozone to climate change) tends to focus on the ozone–temperature relationship (3, 4, 6–9, 16). In this study, we find that a significant impact of VPD variation on the climate–chemistry interaction in the SE during the fall. Under the Representative Concentration Pathway (RCP) 4.5 scenario with a stabilizing CO_2 concentration in the future, the state-of-the-science climate models (e.g., Geophysical Fluid Dynamics Laboratory, GFDL) (Fig. 4*C*) show an increasing trend of daytime VPD ($P < 0.01$). Moreover, the number of high-VPD days, similar to the extreme episodes in 2000 and 2010, is also projected to increase (Fig. 4*D*). In addition, the GFDL model projects an insignificant trend of soil moisture over the SE in October (*SI Appendix*, Fig. S12). This result is consistent with a systematic examination of Coupled Model Intercomparison Project 5 (CMIP5) simulations (38), although the uncertainties in soil moisture projections are large (38). If soil moisture is not the limiting factor, surface ozone will be affected by VPD-regulated biogenic isoprene emissions and it is expected to increase in the future on the basis of the GFDL model projections. In addition, these periods will also likely be accompanied by fewer clouds (more active photochemistry), lower wind speed (less ventilation by advection), and higher temperature (higher biogenic emissions), as in the October 2010 case (Fig. 2*B*), all factors contributing to higher ozone concentrations. The observations in the past three decades indicate that the October ozone extremes in the SE are more sensitive to climate factors than decreasing anthropogenic emissions. Therefore, we suggest that VDP variation is a key factor for understanding the potential of ozone season extension into the fall in the SE in the future in addition to the potential impacts of anthropogenic emission changes. Furthermore, an increase of biogenic isoprene emissions will likely lead to an increase of secondary organic aerosols. Hence, policies effective at mitigating regional climate changes in the SE will also likely reduce the adverse effects of biogenic emissions on regional air quality.

Methods

Ground-Level Ozone Data. We downloaded the hourly ground-level ozone measurements (1980–2010) from the EPA Data Mar (https://aqs.epa.gov/api). To obtain a policy-relevant measure, we first calculated the maximum daily 8-h average ozone ($[O_3]_{MDA8}$) for each site by using hourly data. $[O_3]_{MDA8}$ was used for most of our analysis. To reflect the regional-scale ozone feature, we then averaged over all of the stations within a region (i.e., SE, NE, MW, and CA) to obtain the regional daily $[O_3]_{MDA8}$. To explore the long-term features, we also derived the regional monthly mean $[O_3]_{MDA8}$ by averaging the regional daily $[O_3]_{MDA8}$ within a month. Although the analysis focused on the SE, we also compared results from the SE with those from NE, MW, and CA to better understand the regional differences.

Most of the ozone model-observation comparisons in this study were conducted on a regional basis. By doing so, we reduced the impact of local-scale uncertainties in meteorology and anthropogenic emissions on the comparisons. The SE region, the focus of this study, mainly includes Arkansas, Louisiana, Tennessee, Mississippi, Alabama, Georgia, North Carolina, and South Carolina (Fig. 1*A*). $[O_3]_{MDA8}$ time series at individual sites within a such-defined SE region are well correlated with the regional average (*SI Appendix*, Fig. S13), indicating that the regional average is representative. To ensure the representativeness of the regional average, neighboring states such as Florida, Oklahoma, and Texas are not included in the SE region because of the poor correlations between individual sites in these states and the SE regional average (*SI Appendix*, Fig. S13). In October 2010, however, ozone enhancements also occurred in these states (Fig. 1*A*).

Meteorological Reanalysis Data. We used National Centers for Environmental Prediction Climate Forecast System Reanalysis (CFSR) data (39) to study meteorological patterns associated with regional ozone distributions. The original data were hourly and analyzed meteorological parameters included temperature, relative humidity, and wind speed. To obtain daily measures relevant to ozone production, we derived daily maximum temperature (T_{max}) and daytime-averaged parameters such as RH and wind speed. In this study, daytime is defined as 10:00 AM to 5:00 PM, coincident with the average high-ozone period in a day. We computed daytime-averaged VPD from hourly temperature and RH data. Like ground-level ozone, we derived regional daily and regional monthly-mean series for these meteorological parameters to investigate the regional features on daily and monthly scales, respectively.

Satellite CH_2O Observations. We used satellite formaldehyde column data measured by GOME-2 onboard METOP-A for model comparison (daily retrieval product in 0.25° × 0.25° resolution from h2co.aeronomie.be/) (40). The data are available after 2007. The overpass time for GOME-2 is around 10:00 AM local time. For comparison, model results at the overpass time were sampled. Satellite observations with cloud fraction greater than 40% were removed (40). For Octobers 2008, 2009, and 2010, similar fractions (~50%) of grids are flagged as good quality in the daily retrieval product. For the detailed retrieval algorithm, see De Smedt et al. (40).

Biomass Burning Area and Emissions. We used GFED4s to investigate the impact of fire emissions. GFED combines satellite information on fire activity and vegetation productivity to estimate burned areas (41) and fire emissions (42). The technique described in ref. 43 was applied in GFED4s to include small fires (e.g., fires in croplands and wooded savannas).

Chemical Transport Model Simulations. We used the 3D REAM to explore the missing mechanisms in the biosphere–chemistry–climate interactions. The REAM has been applied over North America, East Asia, and the Polar Regions (24, 25, 44–49). The model has a horizontal resolution of 36 km and 30 vertical layers in the troposphere. Meteorological fields are assimilated by using the Weather Research and Forecasting model constrained by the CFSR data. Transport schemes (advection, convection, and turbulent mixing) are implemented by following previous work (50–52). *SI Appendix*, Fig. S14 shows that the model is able to capture the observations of ozone vertical profile and boundary layer height in Huntsville, AL, reasonably well (nsstc.uah.edu/atmchem/). The anthropogenic emissions are from the emission inventory of 2010 for the Task Force on Hemispheric Transport of Air Pollution version two (HTAPv2, iek8wikis.iek.fz-juelich.de/HTAPWiki/WP1.1). The anthropogenic emission inventory in the United States has been improved greatly in recent years. Therefore, we do not expect large regional biases caused by errors in anthropogenic emissions. The biogenic isoprene emissions are calculated by using the Model of Emissions of Gases and Aerosols from Nature (MEGAN v2.1) algorithm (53), which takes into account emission dependence on physical factors such as temperature, solar radiation, leaf area index, and vegetation functional type. The leaf area index fed into the MEGAN module is from the Moderate Resolution Imaging Spectroradiometer (MODIS, MOD15A2).

The chemical mechanism is adopted from GEOS-Chem v9.1 with updates on chemistry of aromatics (47), isoprene (54, 55), and isoprene nitrates (56–58). It is noteworthy that recent studies (58) found that field measurements are consistent with relatively low NO_x recycling efficiency (~25%), resulting mainly from aerosol uptake, indicating that the impact of isoprene nitrate chemistry on surface ozone is much smaller than previously thought (56). With these updates, we find that the impact of isoprene nitrate chemistry is less than 1 ppbv regionally.

To understand the interannual variation, we conducted 3D REAM simulations for October 2008, 2009, and 2010, which were average, low, and high ozone Octobers, respectively. For the extreme high-VPD and high-ozone October of 2010, a simulation with doubled isoprene emissions reduced the model biases during the episodes, suggesting that the model likely underestimated biogenic emissions during high-VPD periods. To estimate the impact of biomass burning emissions, we conducted model experiments with and without GFED fire emissions. To understand the direct and indirect impact of temperature on ground-level ozone, we also perturbed the boundary layer temperature by +1 K and +2 K with and without the feedback on biogenic isoprene emissions. To compare the sensitivity of daytime ozone to isoprene emissions in the summer and fall, we conducted a base simulation in July 2010 and two sensitivity simulations with 20% enhancement of isoprene emissions in July 2010 and October 2010. We then calculated the relative sensitivity $[(\Delta O_3/O_3)/(\Delta E/E)$ where E is the biogenic emissions] by using the base and sensitivity simulation results.

Climate Model Projections. We obtained climate model forecast from the CMIP5 archive (https://pcmdi.llnl.gov/projects/cmip5/). For comparison with historic daytime VPD, three-hourly outputs of surface temperature and relative humidity were needed to compute the projected daytime VPD. Five

GFDL model outputs under the RCP 4.5 scenario were selected mainly because of the availability of the three-hourly outputs from these model runs. Among these GFDL model runs, only three archived soil moisture.

EVD Method. To interpret the contributions of correlated variables (temperature and VPD) to the ground-level ozone, the EVD method was used. With this method, we decomposed the contributions of temperature and VPD to ground-level ozone (R^2) into that attributable solely to T_{max}, that solely attributable to VPD, and that attributable to the correlation between T_{max} and VPD. See *SI Appendix, SI Text* for detailed description of the method.

ACKNOWLEDGMENTS. We thank Alex Guenther, Roger Seco, Jingqiu Mao, Jenny Fisher, and Katherine Travis for discussion with Y.Z.; and Yongjia Song and Tao Zeng for their help in obtaining and processing the US Environmental Protection Agency (EPA) and reanalysis data. This work was supported by the EPA Science To Achieve Results Programs through Grant RD-83520401.

1. Brunekreef B, Holgate ST (2002) Air pollution and health. *Lancet* 360(9341): 1233–1242.
2. Reich PB, Amundson RG (1985) Ambient levels of ozone reduce net photosynthesis in tree and crop species. *Science* 230(4725):566–570.
3. Jacob DJ, Winner DA (2009) Effect of climate change on air quality. *Atmos Environ* 43(1):51–63.
4. Bloomer BJ, Stehr JW, Piety CA, Salawitch RJ, Dickerson RR (2009) Observed relationships of ozone air pollution with temperature and emissions. *Geophys Res Lett* 36(9):L09803.
5. Leibensperger EM, Mickley LJ, Jacob DJ (2008) Sensitivity of US air quality to mid-latitude cyclone frequency and implications of 1980–2006 climate change. *Atmos Chem Phys* 8(23):7075–7086.
6. Olszyna KJ, Luria M, Meagher JF (1997) The correlation of temperature and rural ozone levels in southeastern U.S.A. *Atmos Environ* 31(18):3011–3022.
7. Steiner AL, et al. (2010) Observed suppression of ozone formation at extremely high temperatures due to chemical and biophysical feedbacks. *Proc Natl Acad Sci USA* 107(46):19685–19690.
8. Fu T-M, Zheng Y, Paulot F, Mao J, Yantosca RM (2015) Positive but variable sensitivity of August surface ozone to large-scale warming in the southeast United States. *Nat Clim Chang* 5(5):454–458.
9. Bloomer BJ, Vinnikov KY, Dickerson RR (2010) Changes in seasonal and diurnal cycles of ozone and temperature in the eastern U.S. *Atmos Environ* 44(21–22):2543–2551.
10. Chen J, et al. (2009) The effects of global changes upon regional ozone pollution in the United States. *Atmos Chem Phys* 9(4):1125–1141.
11. Camalier L, Cox W, Dolwick P (2007) The effects of meteorology on ozone in urban areas and their use in assessing ozone trends. *Atmos Environ* 41(33):7127–7137.
12. Avise J, et al. (2009) Attribution of projected changes in summertime US ozone and PM2.5 concentrations to global changes. *Atmos Chem Phys* 9(4):1111–1124.
13. Nolte CG, Gilliland AB, Hogrefe C, Mickley LJ (2008) Linking global to regional models to assess future climate impacts on surface ozone levels in the United States. *J Geophys Res* 113(D14):D14307.
14. US EPA (2015) National Emissions Inventory (NEI) Air Pollutant Emissions Trends Data. Available at https://www.epa.gov/air-emissions-inventories/air-pollutant-emissions-trends-data. Accessed September 30, 2015.
15. Vukovich FM, Sherwell J (2003) An examination of the relationship between certain meteorological parameters and surface ozone variations in the Baltimore–Washington corridor. *Atmos Environ* 37(7):971–981.
16. Rasmussen DJ, et al. (2012) Surface ozone-temperature relationships in the eastern US: A monthly climatology for evaluating chemistry-climate models. *Atmos Environ* 47(0):142–153.
17. Pegoraro E, et al. (2007) The effect of elevated CO_2, soil and atmospheric water deficit and seasonal phenology on leaf and ecosystem isoprene emission. *Funct Plant Biol* 34(9):774–784.
18. Pegoraro E, et al. (2005) The interacting effects of elevated atmospheric CO_2 concentration, drought and leaf-to-air vapour pressure deficit on ecosystem isoprene fluxes. *Oecologia* 146(1):120–129.
19. Beckett M, et al. (2012) Photosynthetic limitations and volatile and non-volatile isoprenoids in the poikilochlorophyllous resurrection plant *Xerophyta humilis* during dehydration and rehydration. *Plant Cell Environ* 35(12):2061–2074.
20. Potosnak MJ, et al. (2014) Observed and modeled ecosystem isoprene fluxes from an oak-dominated temperate forest and the influence of drought stress. *Atmos Environ* 84(0):314–322.
21. Seco R, et al. (2015) Ecosystem-scale volatile organic compound fluxes during an extreme drought in a broadleaf temperate forest of the Missouri Ozarks (central USA). *Glob Change Biol* 21(10):3657–3674.
22. Zhu J, Liang X-Z (2013) Impacts of the Bermuda High on regional climate and ozone over the United States. *J Clim* 26(3):1018–1032.
23. Shen L, Mickley LJ, Tai APK (2015) Influence of synoptic patterns on surface ozone variability over the eastern United States from 1980 to 2012. *Atmos Chem Phys* 15(19): 10925–10938.
24. Choi Y, et al. (2008) Springtime transitions of NO_2, CO, and O_3 over North America: Model evaluation and analysis. *J Geophys Res* 113(D20):D20311.
25. Zhao C, et al. (2010) Impact of East Asian summer monsoon on the air quality over China: View from space. *J Geophys Res* 115(D9):D09301.
26. Langford AO, Aikin KC, Eubank CS, Williams EJ (2009) Stratospheric contribution to high surface ozone in Colorado during springtime. *Geophys Res Lett* 36(12):L12801.
27. Lin M, et al. (2012) Springtime high surface ozone events over the western United States: Quantifying the role of stratospheric intrusions. *J Geophys Res* 117(D21): D00V22.
28. Lin M, et al. (2015) Climate variability modulates western US ozone air quality in spring via deep stratospheric intrusions. *Nat Commun* 6:7105.
29. Ott LE, et al. (2016) Frequency and impact of summertime stratospheric intrusions over Maryland during DISCOVER-AQ (2011): New evidence from NASA's GEOS-5 simulations. *J Geophys Res, D, Atmospheres* 121(7):3687–3706.
30. Singh HB, Viezee W, Johnson WB, Ludwig FL (1980) The impact of stratospheric ozone on tropospheric air quality. *J Air Pollut Control Assoc* 30(9):1009–1017.
31. Viezee W, Johnson WB, Singh HB (1983) Stratospheric ozone in the lower troposphere—II. Assessment of downward flux and ground-level impact. *Atmos Environ* 17(10):1979–1993.
32. Guenther A, et al. (2006) Estimates of global terrestrial isoprene emissions using MEGAN (Model of Emissions of Gases and Aerosols from Nature). *Atmos Chem Phys* 6(11):3181–3210.
33. Palmer PI, et al. (2003) Mapping isoprene emissions over North America using formaldehyde column observations from space. *J Geophys Res* 108(D6):4180.
34. Shim C, et al. (2005) Constraining global isoprene emissions with GOME formaldehyde column measurements. *J Geophys Res* 110(D24):D24301.
35. Jacob DJ, et al. (1995) Seasonal transition from NO_x- to hydrocarbon-limited conditions for ozone production over the eastern United States in September. *J Geophys Res* 100(D5):9315–9324.
36. Pier PA (1995) Isoprene emission rates from northern red oak using a whole-tree chamber. *Atmos Environ* 29(12):1347–1353.
37. Geron CD, et al. (1997) Biogenic isoprene emission: Model evaluation in a southeastern United States bottomland deciduous forest. *J Geophys Res* 102(15): 18889–18901.
38. Cook BI, Ault TR, Smerdon JE (2015) Unprecedented 21st century drought risk in the American Southwest and Central Plains. *Sci Adv* 1(1):e1400082.
39. Saha S, et al. (2010) The NCEP climate forecast system reanalysis. *Bull Am Meteorol Soc* 91(8):1015–1057.
40. De Smedt I, et al. (2012) Improved retrieval of global tropospheric formaldehyde columns from GOME-2/MetOp-A addressing noise reduction and instrumental degradation issues. *Atmos Meas Tech* 5(11):2933–2949.
41. Giglio L, Randerson JT, van der Werf GR (2013) Analysis of daily, monthly, and annual burned area using the fourth-generation global fire emissions database (GFED4). *J Geophys Res Biogeosci* 118(1):317–328.
42. van der Werf GR, et al. (2010) Global fire emissions and the contribution of deforestation, savanna, forest, agricultural, and peat fires (1997–2009). *Atmos Chem Phys* 10(23):11707–11735.
43. Randerson JT, Chen Y, van der Werf GR, Rogers BM, Morton DC (2012) Global burned area and biomass burning emissions from small fires. *J Geophys Res* 117:G04012.
44. Choi Y, et al. (2008) Spring to summer northward migration of high O_3 over the western North Atlantic. *Geophys Res Lett* 35(4):L04818.
45. Choi Y, et al. (2005) Evidence of lightning NO_x and convective transport of pollutants in satellite observations over North America. *Geophys Res Lett* 32(2):L02805.
46. Gu D, Wang Y, Smeltzer C, Liu Z (2013) Reduction in NO(x) emission trends over China: Regional and seasonal variations. *Environ Sci Technol* 47(22):12912–12919.
47. Liu Z, et al. (2012) Exploring the missing source of glyoxal (CHOCHO) over China. *Geophys Res Lett* 39(10):L10812.
48. Wang Y, et al. (2007) Assessing the photochemical impact of snow emissions over Antarctica during ANTCI 2003. *Atmos Environ* 41(19):3944–3958.
49. Zhao C, Wang Y, Zeng T (2009) East China plains: A "basin" of ozone pollution. *Environ Sci Technol* 43(6):1911–1915.
50. Walcek CJ (2000) Minor flux adjustment near mixing ratio extremes for simplified yet highly accurate monotonic calculation of tracer advection. *J Geophys Res* 105(D7): 9335–9348.
51. Grell GA (1993) Prognostic evaluation of assumptions used by cumulus parameterizations. *Mon Weather Rev* 121(3):764–787.
52. Hong SY, Noh Y, Dudhia J (2006) A new vertical diffusion package with an explicit treatment of entrainment processes. *Mon Weather Rev* 134(9):2318–2341.
53. Guenther AB, et al. (2012) The Model of Emissions of Gases and Aerosols from Nature version 2.1 (MEGAN2.1): An extended and updated framework for modeling biogenic emissions. *Geosci Model Dev* 5(6):1471–1492.
54. Crounse JD, Paulot F, Kjaergaard HG, Wennberg PO (2011) Peroxy radical isomerization in the oxidation of isoprene. *Phys Chem Chem Phys* 13(30):13607–13613.
55. Paulot F, et al. (2009) Unexpected epoxide formation in the gas-phase photooxidation of isoprene. *Science* 325(5941):730–733.
56. Mao J, et al. (2013) Ozone and organic nitrates over the eastern United States: Sensitivity to isoprene chemistry. *J Geophys Res* 118(19):11256–11268.
57. Xiong F, et al. (2015) Observation of isoprene hydroxynitrates in the southeastern United States and implications for the fate of NO_x. *Atmos Chem Phys* 15(19): 11257–11272.
58. Fisher JA, et al. (2016) Organic nitrate chemistry and its implications for nitrogen budgets in an isoprene- and monoterpene-rich atmosphere: constraints from aircraft (SEAC4RS) and ground-based (SOAS) observations in the Southeast US. *Atmos Chem Phys* 16(9):5969–5991.